Journal of Materials Chemistry A

ROYAL SOCIETY OF CHEMISTRY

PAPER

View Article Online
View Journal | View Issue

Cite this: *J. Mater. Chem. A*, 2026, **14**, 1936

Simple additive strategy to boost initial coulombic efficiency by mitigating PTFE decomposition in dry battery electrodes

Hyunji Park[a] and Choongho Yu *[ab]

Received 13th September 2025
Accepted 15th November 2025

DOI: 10.1039/d5ta07497e

rsc.li/materials-a

Dry-processed electrodes eliminate energy/capital-intensive solvent drying processes, but indispensable polytetrafluoroethylene (PTFE) binders suffer from electrochemical reduction by lithium due to the inherently low energy level of their lowest unoccupied molecular orbital (LUMO). We present a strategy to overcome this problem by elevating the LUMO with amine-containing additives, which remove the reduction signature – shoulder in voltage profiles – observed during anode lithiation. The modification, achieved *via* interaction between PTFE's fluorine atoms and the additive's amine group, has been validated by multiple experimental techniques and density functional theory calculations. The additive boosted both initial coulombic efficiency and mechanical durability. Our readily implementable approach involving simple mixing of PTFE with additives opens the door for broader adoption of dry-processed electrodes, addressing one of the most significant impediments in industrialization.

Introduction

With the growth of emerging markets like electric vehicles, the market share of lithium-ion batteries (LIBs) has steadily expanded in recent years. Given this predictable growth, any method that can lower processing or material costs will significantly accelerate the application of LIBs. Among the manufacturing processes of LIBs, electrode production not only directly influences the battery's overall performance but is also one of the most cost-intensive stages, offering considerable potential for cost reduction. In the traditional electrode manufacturing process, polyvinylidene fluoride (PVDF) is commonly used as a binder, dissolved in solvents like *N*-methyl-2-pyrrolidone (NMP). However, due to the high cost of NMP and its toxicity, solvent recovery is required in commercial applications, further increasing the overall cost of battery manufacturing.[1] Regarding the solvent-related aspects during the drying process and recovery, a savings of approximately $36.12 per kW h (a 14.5% reduction) can be achieved based on thin lithium nickel manganese cobalt oxide (NMC) electrodes.[2] Using water instead of toxic NMP offers significant advantages, and for the anode, water-based processes with carboxymethyl cellulose (CMC) and styrene-butadiene rubber (SBR) binders have been developed. However, from an energy perspective, water requires 2260 kJ kg^{-1} to evaporate, more than four times the 510 kJ kg^{-1} required by NMP, making it difficult to consider it the optimal solvent.[1] By eliminating the drying process, the throughput can be increased and energy consumption for heating can be reduced.[3] On top of that, the conventional solvent drying process causes binder migration to the top surface of the electrode.[4,5] The binder gradient induces poor mechanical properties and blocks the pores of the top electrode surfaces, inhibiting the achievement of high-loading electrodes. For these reasons, eliminating solvents from the electrode manufacturing process remains a key objective for manufacturers and an area of significant research interest.[6]

To date, quite a few manufacturing technologies for dry processed films have been reported including dry spraying deposition, 3D printing, melt stretching, powder compression, vapor deposition, and polymer fibrilization.[7] Specifically, the binder fibrillation method is the most promising method due to its feasibility for mass-production with roll-to-roll processes.[8] For the polymer fibrilization method, polytetrafluoroethylene (PTFE) is a widely used binder due to its good mechanical properties, corrosion resistance, and easy fibrilization.[9] Due to high electronegativity of F atoms of PTFE, the repulsive van der Waals force between PTFE molecules is strong, which allows them to slip easily and form PTFE fibrils under shear force.[10] Electrodes using the fibrilized PTFE binder not only have the advantage of a dry process, but also have better electrical properties with their low tortuosity compared to conventional slurry-cast electrodes. Unlike wet-processed binders, which cover the surface of the active material, PTFE, which binds particles with its fibrils, does not block the surface and has a lower charge transfer resistance, facilitating fast charging.[11]

However, PTFE has an intrinsic problem of being easily reduced by reacting with lithium due to its low energy level of

[a]*Department of Mechanical Engineering, Texas A & M University, College Station, Texas 77843, USA. E-mail: chyu@tamu.edu*

[b]*Department of Materials Science and Engineering, Texas A & M University, College Station, Texas 77843, USA*

the lowest unoccupied molecular orbital (LUMO).[12,13] As the following phenomenon occurs, reductive defluorination of PTFE takes place, with the detached fluorine reacting with lithium to form LiF, while the remaining PTFE can either leave behind carbyne-like carbon[14–16] or be terminated by hydrogen.[12,17]

$$(CF_2)_n + 2nLi^+ + 2ne^- \rightarrow (C{\equiv}C)_n + 2nLiF \quad (1)$$

If this reaction occurs stoichiometrically, 1072 mA h of lithium is consumed per gram of PTFE (see note S1), which could lead to significant capacity drop. In particular, the anode exhibits inferior initial coulombic efficiency (ICE) due to the reduced binder and experiences noticeable capacity decay as a result of brittleness caused by degraded mechanical properties.[17–19] According to the news reports on Tesla's dry battery electrodes low ICE in the anode presents challenges for commercialization. However, developing alternative materials that fiberize easily and offer greater electrochemical stability than PTFE remains challenging.

An attempt to minimize PTFE content has been reported, but this is not a definitive solution and involves a trade-off with mechanical properties, which are closely tied to thickness variations.[11,20] Very recently, mitigating reduction of PTFE by coating the graphite active material with insulating polymers was proposed to mitigate the electrochemical degradation of PTFE and thereby undesirable lithium loss.[12,21] However, the coating process of graphite particles still requires a wet process involving a solvent. More importantly, wet coating of insulating binders on the active material diminishes the advantages of the fibrous binders by minimizing their contact areas.

Herein, we propose a strategy to mitigate the inherent challenge of PTFE reduction by modulating its LUMO with additives to suppress its electrochemical decomposition. A key additive is tyramine (Ty), which contains an amine group capable of forming hydrogen bonds with PTFE through a solvent-free mixing process. In PTFE, the LUMO originates from antibonding combinations of the C 2s and C $2p_y$ orbitals, along with mixed F $2p_x$ orbitals having anti-bonding character in the C–F bond.[22,23] Hydrogen bonding can influence the electron density and enable engineering of the band structure.[24–26] When the amine group interacts with PTFE, it redistributes electron density, thereby modulating the electronic band structure. This was confirmed by density functional theory (DFT) calculations as well as experimental results from ultraviolet-visible (UV-Vis) spectroscopy and ultraviolet photoelectron spectroscopy (UPS). The dry-processed anode with the pristine PTFE binder exhibited a low ICE of 91.6%, indicating PTFE reduction in the first lithiation profile of the graphite half-cell. In contrast, PTFE with tyramine (PTFE@Ty) suppressed the electrochemical degradation of PTFE, increasing the ICE to 94.4%. The full cell with the additive also demonstrated improved ICE and capacity retention, achieving higher specific capacities than the PTFE electrode without the additive. The electrochemical decomposition of PTFE in the absence of the additive led to fiber breakage and increased the electrode thickness, adversely affecting the cycle performance. To the best of our knowledge, this work represents the first attempt to tune the LUMO of PTFE to avoid its electrochemical degradation. This approach paves the way for mitigating the reduction of fibrous PTFE binders and enabling high energy-density, cost-effective lithium-ion batteries.

Results and discussion

Role of additives in modifying the electronic bands of PTFE

The inherently low LUMO level of PTFE, which lies below the Fermi level of Li metal, is the primary cause of its electrochemical decomposition. Therefore, raising the LUMO level can help mitigate this issue. Band structures can be altered through approaches like chemical doping, interatomic interactions, and mechanical strain.[27–30] Specifically, by incorporating new bonds such as covalent bonds and hydrogen bonds, the electronic structure can be adjusted. Introducing electron-donating functional groups like methoxy or amino groups enhances electron density, thereby elevating the LUMO level.[31,32] Utilizing an additive to form a hydrogen-bonded complex allows for modulating the electronic structure without necessitating new synthesis methods.[24,25,33,34] The redistribution of orbitals depends on the neighboring atoms and the extent of polarization in the hydrogen bond, which influences whether the LUMO and HOMO of the complex are lowered or raised in energy.[34,35] Enhancing the donor/acceptor characteristics facilitates charge transfer interactions, allowing for the reorganization of orbitals.[24,25,33,34]

Specifically, the C–F groups establish relatively robust intermolecular hydrogen bonds with amine groups.[36] Tyramine (1-hydroxy-4-ethylaminobenzene, Ty) is a naturally occurring organic nitrogenous compound found in food, valued for its simple synthesis, low cost, and broad range of applications. The amine group of tyramine can form hydrogen bonds with the fluorine atoms in PTFE.[37] The C–F groups in PTFE, protected by amine groups, may also alleviate direct contact with conducting materials, thereby minimizing the electrochemical decomposition of PTFE (Fig. 1(a)). As shown in Fig. 1(b), DFT calculations showed that the binding energy of PTFE and Ty is 0.155 eV and their distance is 3.427 Å, which are within the range of hydrogen bonds.[38,39] According to the DFT calculation results, the LUMO level of PTFE interacting with tyramine is increased by 0.249 eV due to the interaction (Fig. S2, S3 and Table S1). The HOMO of the PTFE–Ty complex originates from Ty while the LUMO is primarily from PTFE. Similarly, we explored whether small molecules with amine groups, such as melamine and benzimidazole, could form interactions similar to those of Ty. Both melamine and benzimidazole exhibit a binding energy of 0.1 eV and an intermolecular distance in the range of 2.5–3 Å.

Taking into account the binding energy and LUMO level, we selected Ty for further experiments to determine the LUMO of the PTFE/Ty complex (PTFE@Ty). First, UPS was carried out to examine the HOMO level, while the band gap was measured using UV-Vis spectroscopy (Fig. 1(c–e), S4 and S5). The HOMO (E_{HOMO}) levels were calculated using the equation, $|E_{HOMO}| = |h\nu - (E_{cutoff} - E_{onset})|$, where E_{cutoff} represents the intersection of the sloping line and the baseline, E_{onset} corresponds to the binding energy at the onset of the spectra, and $h\nu$ denotes the energy of

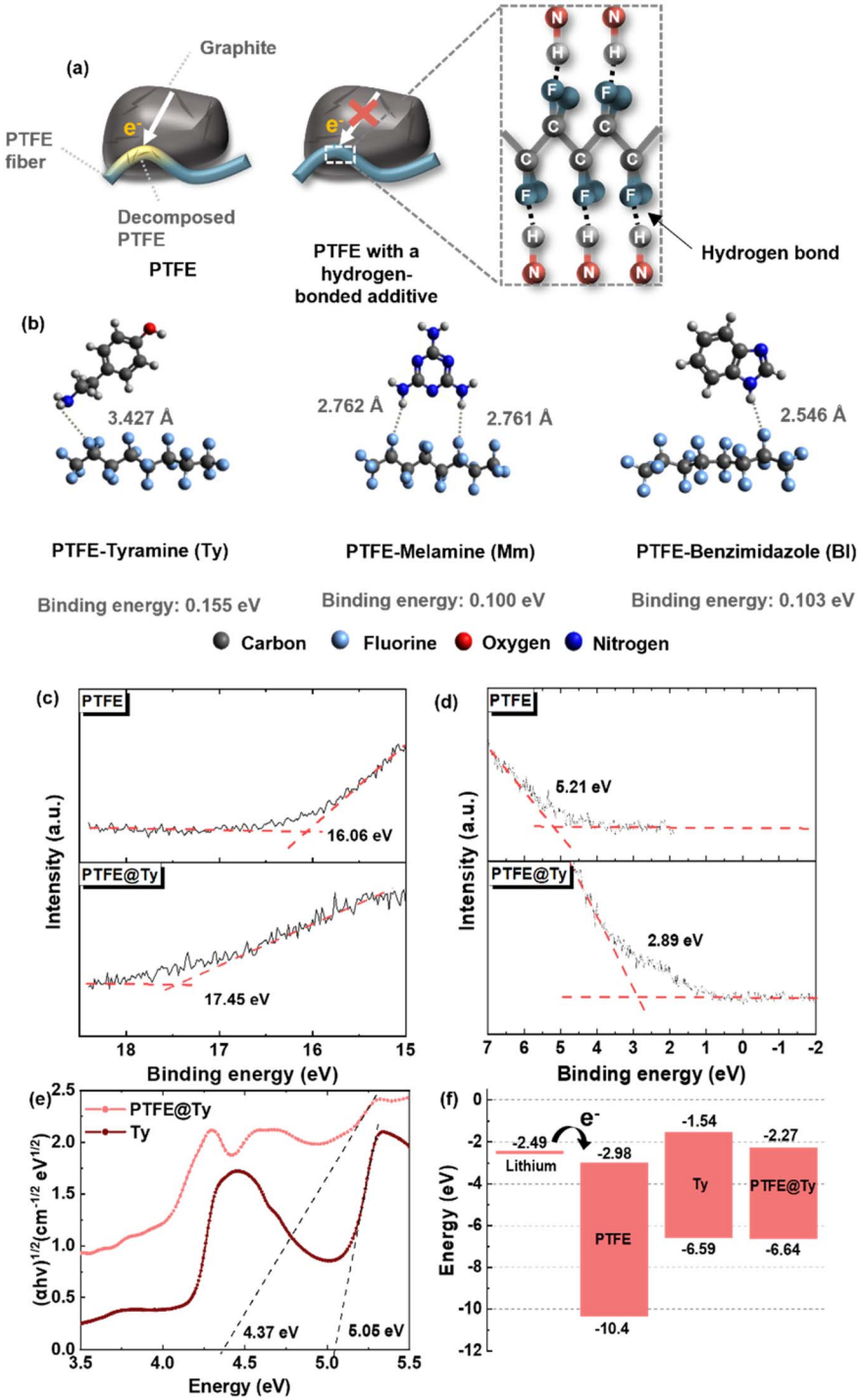

Fig. 1 Modification of LUMO and HOMO levels in PTFE upon coupling with tyramine to form the PTFE–tyramine complex (PTFE@Ty). (a) Illustration of a fibrous PTFE binder in a dry-processed anode with or without the Ty additive. (b) Optimized configurations and binding energies of PTFE–tyramine, PTFE–melamine, and PTFE–benzimidazole. (c) Cutoff region and (d) the onset region of the UPS spectra for PTFE and PTFE@Ty (2 : 1 wt%). (e) Tauc plots showing the band gap derived from the UV-Vis spectra. (f) Energy level diagram of PTFE, tyramine, and PTFE@Ty, constructed based on the UPS and UV-Vis results.

the incident photon from the He I source (21.2 eV).[40,41] Based on the UPS measurements, the E_{HOMO} values for PTFE and PTFE@Ty were determined to be 10.4 eV and 6.64 eV, respectively. The HOMO level of PTFE is consistent with those in the literature.[22,42] To locate the LUMO level of PTFE@Ty, the band gap was determined by UV-Vis spectroscopy using the Tauc plot with the equation, $(\alpha h\nu)^n = A(h\nu - E_g)$, where α is the absorption coefficient, n is 2 for indirect allowed transitions, A is a constant, and E_g represents the band gap. Given PTFE's large band gap, we adopted the previously reported band gap of 7.66

eV obtained using vacuum UV spectroscopy.[22,43] As depicted in Fig. 1(f), the experimental results indicate that Ty raises the LUMO level of PTFE beyond the work function of lithium (2.49 eV),[44,45] suggesting that PTFE in combination with Ty can effectively mitigate PTFE reduction.

To assess its stability, solubility tests followed by UV-Vis spectroscopy were carried out to see whether tyramine dissolves in a carbonate-based electrolyte, which is commonly employed in LIBs. The electrode consisting of the PTFE@Ty complex and graphite did not exhibit noticeable peaks corresponding to tyramine in dimethyl carbonate solvent, whereas Ty itself primarily precipitated due to its low solubility (Fig. S6). Furthermore, identical linear sweep voltammetry measurements performed both with and without tyramine within the operating voltage range of LIBs validated its electrochemical stability, showing no significant redox reactions (Fig. S7). The thermal stability of the PTFE@Ty system is supported by the melting point of tyramine (163 °C) and UPS measurements performed after hot calendaring at 80 °C, which confirm that the functional properties of the composite are preserved. Given that typical electrode processing (~40–80 °C) and operating temperatures are below this temperature, the PTFE@Ty system can be considered thermally stable under practical conditions.

Interactions between PTFE and Ty

The PTFE used consists of elliptical-shaped particles with fibrous structures in between, while tyramine particles ranged from tens to hundreds of nanometers up to several microns, with larger particles exhibiting a layered structure, as observed in scanning electron microscopy (SEM) images (Fig. S8 and S9). Dry mixing PTFE and tyramine under shear force increased fiber formation, with some fibers clustering into a film-like structure (Fig. S10). As shown in Fig. 2(a), energy-dispersive X-ray spectroscopy (EDS) mapping results reveal that nitrogen in tyramine is evenly distributed rather than clustered with slightly higher densities in the regions where *F* in PTFE is present. This may suggest that the mixing process disrupted intermolecular pi–pi interactions between benzene rings in tyramine, breaking it down to small fragments and likely facilitating hydrogen bond formation throughout PTFE. The extent of PTFE reduction depends on the degree of fibrillation, as the exposed PTFE surface directly affects the reduction reaction. It is therefore important to evaluate whether tyramine may interfere with the fibrillation process. As displayed in the SEM image of a dry-processed anode composed of PTFE@Ty and graphite, PTFE@Ty exhibits fibrous morphologies similar to those of pristine PTFE, forming long fibers with diameters ranging from tens to hundreds of nanometers, highlighting its effective role as a binder (Fig. 2(b) and S11). If fibrillation was insufficient, poor electronic pathways and increased interfacial resistance would have led to a higher charge-transfer resistance.[46,47] However, the PTFE@Ty electrode with the optimized amount exhibited a comparable resistance (Fig. S12), implying that the fibrillation network was well preserved.

The interactions between dry-mixed PTFE and Ty were observed by Fourier transform infrared (FT-IR) spectroscopy and X-ray photoelectron spectroscopy (XPS). The PTFE peaks corresponding to the symmetric and asymmetric stretching vibrations of C–F_2 at 1142.7 and 1201.5 cm^{-1} were blue-shifted to 1148.2 and 1202.6 cm^{-1}, respectively, for the blending weight ratio of PTFE to tyramine of 5 : 1 (Fig. 2(c)). The magnitude of the peak shift was less pronounced for the lower Ty content in PTFE@Ty (10 : 1) compared to PTFE@Ty (5 : 1). This suggests that a higher tyramine content enables greater coverage of C–F sites in PTFE. The wagging vibration peaks at 637.4 cm^{-1} and 623.9 cm^{-1} also exhibited blue shifts.[48,49] These results could be attributed to a reduction in C–F bond lengths of PTFE due to the interactions between Ty and PTFE, as confirmed from DFT results (Fig. S11). The peak at 553.6 cm^{-1}, corresponding to bending vibrations, overlaps with the peak of Ty, making it difficult to discern the peak shift (Fig. S14). Consistent with FT-IR results in Fig. 2(c), XPS peaks corresponding to C–F_2 in both C 1s and F 1s spectra were also observed to shift toward higher energy. When calibrated with C–C at 284.5 eV, the peak corresponding to C–F_2 in the C 1s spectra shifted from 291.1 eV to 291.9 eV with tyramine (PTFE@Ty (5 : 1)). Similarly, in the F 1s spectrum, a peak shift from 688.4 eV to 689.1 eV was observed. These shifts toward higher energy in the XPS spectra suggest changes in the electronic environment of the PTFE due to interactions with tyramine, indicating a reduction in electron density around the C–F bonds. This is consistent with the hypothesis that tyramine interacts with and modifies the surface of PTFE, resulting in stronger binding of C–F sites by tyramine. Collectively, the FT-IR and XPS data provide robust confirmation of the chemical modifications occurring at the PTFE surface, underscoring the role of tyramine in altering the material's properties.

Electrochemical performance

The reduction of PTFE by lithium is evidenced by changes in the voltage profile and a decrease in ICE. In the half-cell tests (Fig. 3(a, b) and S15), the shoulder feature in the voltage profile, attributed to the electrochemical decomposition of 5 wt% PTFE, is distinctly observed at ~0.7 V. This decomposition results in a lower delithiation capacity and a reduced ICE of 87%. When the PTFE content was reduced to 2 wt%, the voltage shoulder became less prominent due to the reduced amount of material available for the side reactions. However, compared to the wet-processed electrode lacking PTFE, a slight shoulder remained. In contrast, the incorporation of 0.4 wt% tyramine (PTFE@Ty) mitigated this undesirable effect, yielding a voltage profile comparable to that of a conventional anode fabricated using the wet slurry method with CMC/SBR binders. Notably, tyramine did not introduce any adverse effects, such as unwanted side reactions or increased resistance leading to higher overpotential. Consequently, the ICE of PTFE@Ty improved to 94.4%, compared to 91.6% in the absence of tyramine. To verify the general applicability of the proposed approach, the effect of tyramine was further investigated using various electrolytes, including commercial formulations (Fig. S16). In all tested systems, the characteristic voltage shoulder associated with PTFE degradation during the initial charge/discharge process disappeared, accompanied by a consistent improvement in ICE. These results confirm that the beneficial effect of tyramine is not electrolyte-dependent. Based on the

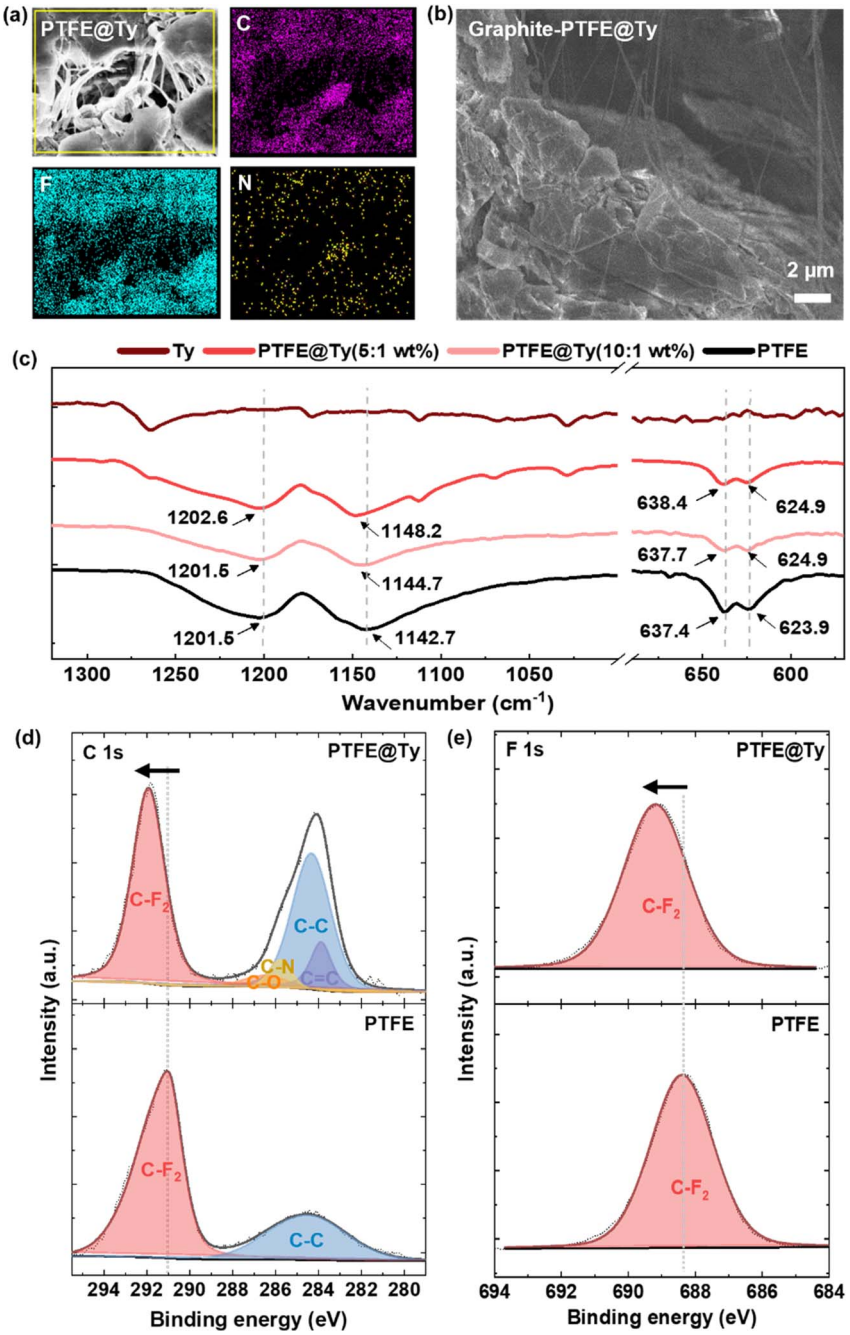

Fig. 2 Experimental results on the interactions between PTFE and tyramine. (a) SEM and EDS images of PTFE@Ty (5 : 1). (b) SEM image of an anode consisting of graphite (95 wt%) and the PTFE@Ty (5 : 1) binder (5 wt%). (c) FT-IR spectra showing symmetric and asymmetric stretching vibrations of C–F_2 and wagging vibrations of C–F_2. XPS results of PTFE or PTFE@Ty (5 : 1) corresponding to (d) C 1s and (e) F 1s spectra.

initial electrolyte screening, the electrolyte yielding the highest ICE was selected for subsequent electrochemical evaluations.

While reducing the PTFE content enhances ICE, it can lead to poor cycling performance, meaning it cannot be reduced indefinitely. At 5 wt%, both PTFE and PTFE@Ty exhibited good cycling stability, whereas at 2 wt%, the half-cell cycle life declined slightly, and at 1 wt%, it became significantly inferior (Fig. 3(c) and S17). This is because PTFE degradation compromises its ability to effectively function as a binder. In the full cells made of the $LiNi_{0.8}Mn_{0.1}Co_{0.1}O_2$ (NMC 811) cathode and natural graphite anode (Fig. 3(d) and S18), the capacity retention with 2 wt% PTFE was suboptimal likely due to a limited supply of lithium compared to half cells. However, we noticed that integrating carbon nanotubes (CNTs) enhances the cycle life. After 50 cycles, the PTFE cell retained 78% of its initial capacity, which increased to 85% with CNTs. With the incorporation of Ty into PTFE, the retention further improved to 95% with CNTs. We believe the fibrous CNT network not only provides the structural reinforcement to PTFE fibers, alleviating the capacity drop caused by mechanical degradation, but also

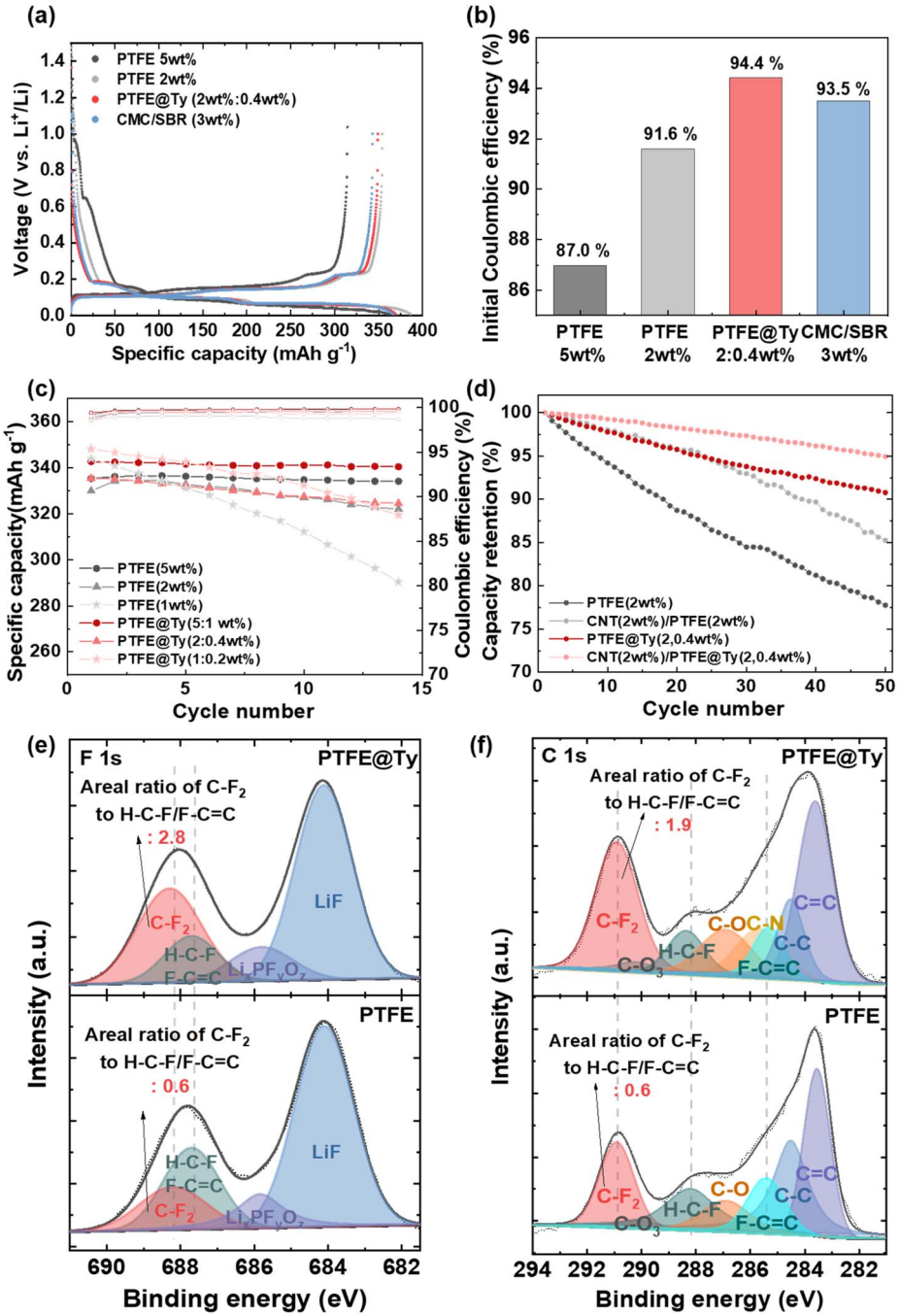

Fig. 3 (a) Initial lithitation/delithiation profiles of half cells consisting of natural graphite with the PTFE (5 and 2 wt%) or PTFE@Ty (2, 0.4 wt%; the first number refers to the PTFE content, and the second number refers to the tyramine content in the total electrode mass.) binder along with wet-processed electrodes containing CMC/SBR binder (3 wt%) at 0.05C. (b) Corresponding ICE of the half cells in 'a'. (c) Cycle performances (0.3C) of half cells using natural graphite depending on PTFE content and the inclusion of Ty. (d) Effects of CNTs on the capacity retention of full cells (NMC811/natural graphite) at 0.3C. XPS analyses for (e) F 1s and (f) C 1s spectra of the half-cell electrodes with 2 wt% PTFE, with and without tyramine after the first cycle at 0.05C at the fully delithiated state.

enhances electrical conductivity.[50–55] It appears that preventing structural degradation also curtails electrochemical side reactions that consume reversible lithium. Based on both ICE and capacity retention, further experiments were performed using both PTFE and CNTs.

We also performed XPS measurements after the first cycle at the fully delithiated state (Fig. 3(e and f)). In the F 1s spectra, besides the C–F_2 peak corresponding to PTFE, a H–C–F/F–C=C peak was observed, indicating that the defluorination of C–F_2 could produce H–C–F or a carbyne structure such as F–C=C.[12,19] Since LiF primarily originates from the solid electrolyte interface layer formed by $LiPF_6$ in the electrolyte, these findings could suggest electrochemical degradation of the binder. Here tyramine effectively maintained the larger areal ratio of the C–F_2

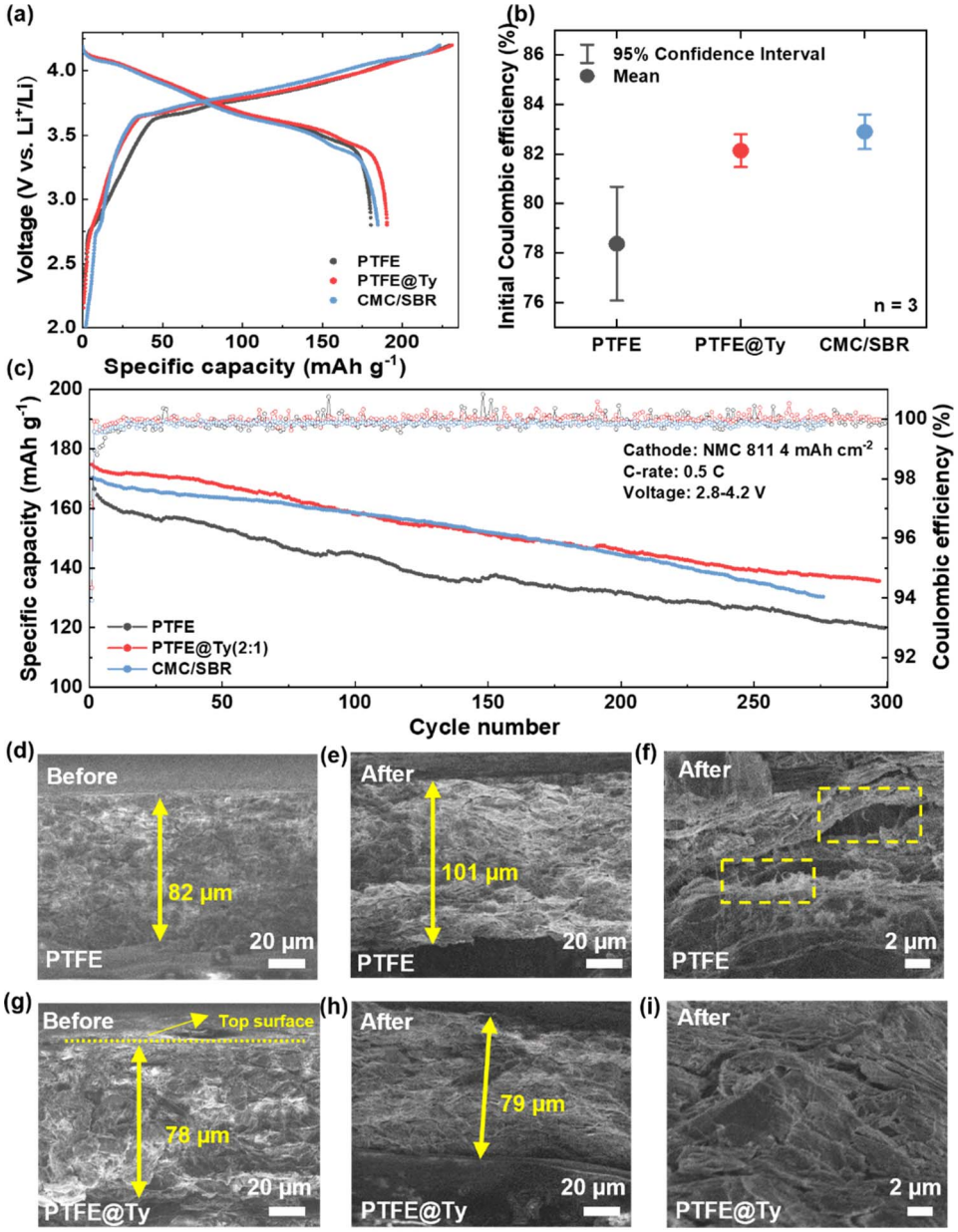

Fig. 4 Electrochemical performances of full cells consisting of conventional wet-processed $LiNi_{0.8}Mn_{0.1}Co_{0.1}O_2$ cathodes paired with one of the three different artificial graphite anodes – dry-processed PTFE (2 wt%) and PTFE@Ty (2, 1 wt%) binders, and a wet-processed CMC/SBR (3 wt%) binder. (a) Initial charge/discharge profiles recorded at 0.05C. (b) Comparison of ICE for the full cells in 'a'. (c) Cycling performances of the full cells at 0.5C with 4 mA h cm^{-2} areal capacity. Reproducibility data are provided in Fig. S20. Cross-sectional SEM images of the anodes in 'c' with (d) PTFE and (g) PTFE@Ty binders before cycling; and those with ((e) and (f)) PTFE and ((h) and (i)) PTFE@Ty after 300 cycles at the fully discharged state.

peak relative to the H–C–F/F–C=C peak in PTFE, demonstrating a substantial suppression of the electrochemical decomposition of the binder. Tyramine enlarged the C–F_2 peak area by 4.7 times with the absolute areal ratio of C–F_2 to H–C–F/F–C=C reaching 2.8 (normalized: 74%) for PTFE@Ty, compared to 0.6 (normalized: 38%) for PTFE. Similarly, in the C 1s spectra, the C–F_2 peak for PTFE@Ty remained significantly larger than the H–C–F and F–C=C peaks, with an areal ratio of C–F_2 to H–C–F/F–C=C reaching 1.9 (normalized: 65%), compared to 0.6 (normalized: 38%) for PTFE. Although tyramine and PTFE were thoroughly mixed, some unreacted PTFE regions are unavoidable, as inner PTFE exposed during additional fibrillation with graphite may not fully interact with tyramine. Consequently, while minor H–C–F/F–C=C features remained, the overall defluorination was significantly suppressed compared to the pristine PTFE electrode. In addition, electrochemical impedance spectroscopy (EIS) analysis further supports this conclusion by demonstrating suppressed interfacial reactions for PTFE@Ty. Both the solid electrolyte interphase (SEI) resistances and charge-transfer resistances

remained substantially lower than those of pristine PTFE after formation cycling (Fig. S19), indicating that hydrogen-bond-assisted LUMO elevation effectively mitigates PTFE reduction. These results confirm that the enhancement in ICE was directly attributable to the Ty's ability to prevent PTFE decomposition.

We also carried out full-cell tests with wet-processed NMC 811 cathodes (Fig. S20). To assess the impact of the PTFE-to-Ty ratio in a full cell configuration, we tested weight ratios of 5 : 1, 2 : 1, and 1 : 1 while keeping the PTFE content fixed at 2 wt% (Fig. S21–S23). The 2 : 1 ratio resulted in a greater increase in ICE compared to the 5 : 1 ratio, but the further increase of tyramine (1 : 1 ratio) slightly reduced the ICE. The discharge capacity of the 2 : 1 case was considerably higher than that of the 1 : 1 ratio and comparable to the 5 : 1 ratio. While an optimal amount of tyramine effectively mitigates PTFE decomposition and enhances ICE, excessive tyramine may increase resistance, leading to capacity loss. As shown in the EIS data (Fig. S11), the 2 : 1 ratio exhibited similar interfacial resistance compared to pristine PTFE, whereas the 1 : 1 ratio showed noticeably higher resistance. Therefore, the PTFE-to-Ty weight ratio of 2 : 1 was selected for further testing in the full cell.

The PTFE case (2 wt%) exhibited a distinct first-charge voltage profile compared to PTFE@Ty and CMC/SBR cases (Fig. 4(a)), consistent with the half-cell results. It also showed a lower ICE than those of the other two cases due to lithium loss associated with PTFE reduction (Fig. 4(b)). PTFE@Ty demonstrated a lifespan comparable to that of wet-processed anodes using CMC/SBR binders, confirming its effectiveness as a binder (Fig. 4(c), S24, and S25). After 300 cycles at 0.5C, PTFE@Ty retained 77.7% of its capacity, whereas PTFE retained 70.6%. EIS measurements show that both SEI and charge-transfer resistances of PTFE@Ty remain lower than those of pristine PTFE even after long-term cycling, maintaining enhanced interfacial stability and effective suppression of PTFE decomposition (Fig. S26). More importantly, the inclusion of tyramine substantially suppressed electrode swelling, a critical factor in practical battery operation, as excessive swelling can lead to pouch or can failure and fracture. As shown in the cross-sectional image of Fig. 4(d–f), the thickness of the PTFE electrode expanded from approximately 82 μm to 101 μm after 300 cycles, whereas PTFE@Ty exhibited a notably smaller increase, reaching 79 μm (Fig. 4(g–i)). This suggests that PTFE, due to defluorination, was less proficient as a binder, leading to an inability to accommodate the anode's volume changes during charge–discharge cycles, which contributed to a further decline in capacity retention during the initial cycles. In contrast, PTFE@Ty maintained minimal gaps between graphite particles even after 300 cycles, with the binder fibers remaining intact and well-preserved.

Moreover, the dry-processed anode demonstrated superior rate performance compared to the wet-processed anode, with the difference being more pronounced at the high current density of 2C (Fig. 5(a) and S27). This difference was investigated using the galvanostatic intermittent titration technique (GITT) in half cells as well as EIS in symmetric cells. In the GITT graph, PTFE@Ty exhibits an initial behavior similar to that of

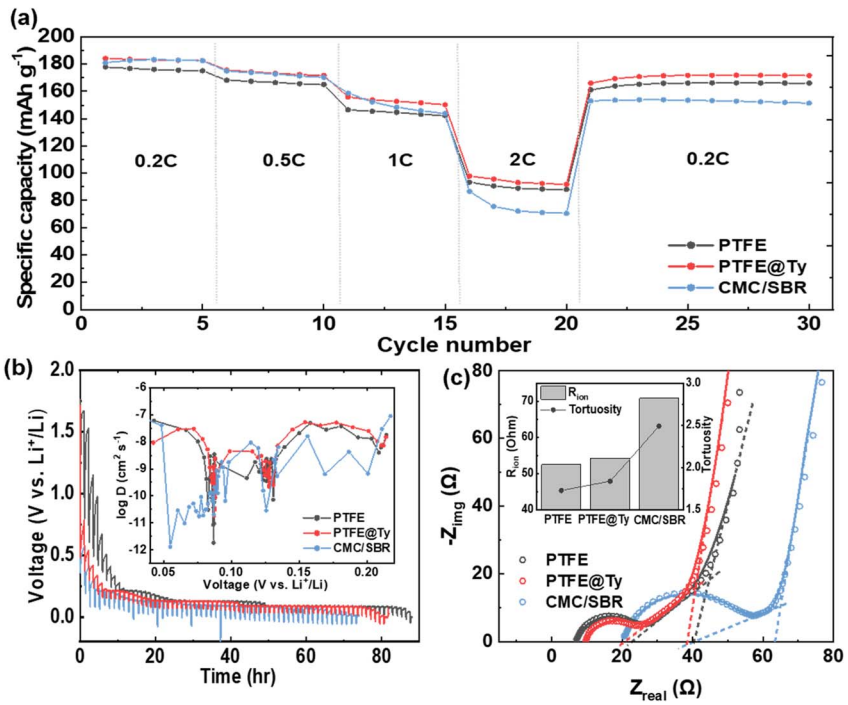

Fig. 5 (a) Rate capability of full cells consisting of 4 mA h cm^{-2} $LiNi_{0.8}Mn_{0.1}Co_{0.1}O_2$ cathodes and artificial graphite anodes using PTFE (2 wt%), PTFE@Ty (2, 1 wt%), or CMC/SBR (2 wt%) binders at C-rates ranging from 0.2 to 2C. (b) Galvanostatic intermittent titration-technique (GITT) test during the first lithiation process. The inset represents logarithmic values of the calculated diffusion coefficients from the GITT as a function of voltage. (c) Bar graphs of R_{ion} and tortuosity obtained from the EIS data of symmetric cells with anodes prepared with PTFE (2 wt%), PTFE@Ty (2, 1 wt%), or CMC/SBR (2 wt%) binders. The corresponding EIS Nyquist plots of symmetrical cells are shown in the inset.

the wet-processed anode without the shoulder due to PTFE decomposition. Fig. 5(b) and S28 presented the calculated Li^+ diffusion coefficients in the corresponding potential range (0.05–0.25 V) during lithium insertion into graphite, indicating improved Li^+ diffusion on the graphite surface in the dry-processed anode compared to the wet-processed anode. Furthermore, the R_{ion} and tortuosity values obtained from EIS of the dry-processed anodes were lower than those of conventional wet-processed anodes, enabling more effective lithium-ion transport (Fig. 5(c) and Table S2). As confirmed in several studies,[11,56] the fibrous PTFE binder does not obstruct the graphite surface, thus enhancing the dynamic behavior of lithium ions. With the Ty additive, these properties were further improved owing to the diminished side reactions in PTFE. The slightly higher ionic resistance observed for PTFE@Ty is likely due to the surface modification of the binder by the tyramine additive, which marginally increases the tortuosity of ion pathways within the electrode. However, this effect is minor and does not significantly hinder overall ion transport. In contrast, the charge-transfer resistance obtained from EIS measurements after formation cycles (Fig. S19) was lower for PTFE@Ty than for pristine PTFE, indicating that the suppression of PTFE reduction leads to enhanced interfacial stability and improved reaction kinetics. Consequently, the minor increase in ionic resistance is compensated by the improved charge-transfer behavior, resulting in an overall enhancement in the electrochemical performance.

Elevating the LUMO level in this manner offers a readily deployable solution to the electrochemical degradation of PTFE, in contrast to earlier methods such as coating active materials with solvents exhibiting reduced conductivity (Table S3). Our approach achieves this objective without employing any solvents, thereby upholding the goal of eliminating solvent usage and energy/capital-intensive evaporation processes. Tyramine, a naturally derived amine commonly found in protein-rich foods and biological systems, is abundantly available and easily synthesized from inexpensive precursors, making it cost-effective and readily accessible. Its cost is comparable to that of commonly used polymer binders, indicating that it can serve as a cost-effective additive without adding significant material expense. Moreover, as it safeguards the surface of PTFE rather than the active material, it is more effectively applicable to various electrolytes and anode materials. To the best of our knowledge, this is the first endeavor to raise the LUMO of PTFE, which is expected to accelerate the commercialization of more affordable, high-energy-density dry-processed batteries.

Conclusion

We have demonstrated that the electrochemical decomposition of the PTFE binder can be avoided by a readily deployable method – incorporating additive molecules bearing amine groups. The additive elevates the inherently low LUMO of PTFE, making it less prone to electron acceptance, as validated using both experimental (UPS and UV-Vis) and theoretical (DFT) results. The interaction between PTFE and Ty was supported by the DFT calculations and confirmed experimentally by FT-IR and XPS analyses. The additive boosted the ICE in half cells from 91.6% to 94.4%, as evidenced by removal of the voltage shoulder caused by the side reactions of PTFE. This mitigated unnecessary lithium loss and degradation of the PTFE binder during lithiation, consequently enhancing the initial discharge capacity and capacity retention in NMC 811/graphite full cells. After 300 cycles at 0.5C, PTFE@Ty retained 77.7% of its initial capacity, compared to 70.6% for PTFE alone, demonstrating cycling performance comparable to that of wet process electrodes. This approach addresses a major bottleneck in the development of dry processed electrodes, paving the way for high loading, low-cost, and environmentally friendly fabrication.

Author contributions

Hyunji Park: conceptualization, investigation, software, data curation and writing – original draft. Choongho Yu: conceptualization, supervision, writing – review & editing.

Conflicts of interest

There are no conflicts to declare.

Data availability

The data supporting this article have been included as part of the supplementary information (SI). Supplementary information: detailed descriptions of the experimental procedures and computational methods used in this study; additional characterization data obtained from UPS, UV-Vis, LSV, SEM, FT-IR, and EIS, as well as charge–discharge profiles, coulombic efficiency, and dQ/dV analyses; procedures for calculating tortuosity and the method used to estimate the capacity loss associated with PTFE reduction. See DOI: https://doi.org/10.1039/d5ta07497e.

References

1 D. L. Wood, J. D. Quass, J. Li, S. Ahmed, D. Ventola and C. Daniel, *Dry. Technol.*, 2018, **36**, 234–244.
2 D. L. Wood III, J. Li and C. Daniel, *J. Power Sources*, 2015, **275**, 234–242.
3 Y. Lu, C.-Z. Zhao, H. Yuan, J.-K. Hu, J.-Q. Huang and Q. Zhang, *Matter*, 2022, **5**, 876–898.
4 M.-W. von Horstig, A. Schoo, T. Loellhoeffel, J. K. Mayer and A. Kwade, *Energy Technol.*, 2022, **10**, 2200689.
5 J. Klemens, L. Schneider, E. C. Herbst, N. Bohn, M. Müller, W. Bauer, P. Scharfer and W. Schabel, *Energy Technol.*, 2022, **10**, 2100985.
6 W. Jin, G. Song, J. K. Yoo, S. K. Jung, T. H. Kim and J. Kim, *ChemElectroChem*, 2024, e202400288.
7 Y. Li, Y. Wu, Z. Wang, J. Xu, T. Ma, L. Chen, H. Li and F. Wu, *Mater. Today*, 2022, **55**, 92–109.
8 J. Park, J. Kim, J. Kim, M. Kim, T. Song and U. Paik, *Chem. Sci.*, 2025, **16**, 6598–6619.

9 X. Wang, S. Chen, K. Zhang, L. Huang, H. Shen, Z. Chen, C. Rong, G. Wang and Z. Jiang, *Materials*, 2023, **16**, 7232.
10 K. Sato, Y. Tominaga, Y. Imai, T. Yoshiyama and Y. Aburatani, *Polym. Test.*, 2022, **113**, 107690.
11 Y. Suh, J. K. Koo, H.-j. Im and Y.-J. Kim, *Chem. Eng. J.*, 2023, **476**, 146299.
12 Z. Wei, D. Kong, L. Quan, J. He, J. Liu, Z. Tang, S. Chen, Q. Cai, R. Zhang, H. Liu, K. Xu, L. Xing and W. Li, *Joule*, 2024, **8**, 1350–1363.
13 N.-S. Choi, S.-Y. Ha, Y. Lee, J. Y. Jang, M.-H. Jeong, W. C. Shin and M. Ue, *J. Electrochem. Sci. Technol.*, 2015, **6**, 35–49.
14 L. Kavan, *Chem. Rev.*, 1997, **97**, 3061–3082.
15 G. Li, R. Xue and L. Chen, *Solid State Ionics*, 1996, **90**, 221–225.
16 S. Shiraishi, T. Kobayashi and A. Oya, *Chem. Lett.*, 2005, **34**, 1678–1679.
17 J. Lee, C. Y. Son, S. Han, S. Yang, P. J. Kim, D. Lee, J. W. Lee, W.-H. Ryu and J. Choi, *Chem. Eng. J.*, 2024, 158271.
18 Y. Zhang, F. Huld, S. Lu, C. Jektvik, F. Lou and Z. Yu, *Batteries*, 2022, **8**, 57.
19 S. Han, E.-H. Noh, S. Chae, K. Kwon, J. Lee, J.-S. Woo, S. Park, J. W. Lee, P. J. Kim and T. Song, *J. Energy Storage*, 2024, **96**, 112693.
20 D. J. Lee, J. Jang, J. P. Lee, J. Wu, Y. T. Chen, J. Holoubek, K. Yu, S. Y. Ham, Y. Jeon and T. H. Kim, *Adv. Funct. Mater.*, 2023, 2301341.
21 T. Lee, J. An, W. J. Chung, H. Kim, Y. Cho, H. Song, H. Lee, J. H. Kang and J. W. Choi, *ACS Appl. Mater. Interfaces*, 2024, **16**, 8930–8938.
22 K. Seki, H. Tanaka, T. Ohta, Y. Aoki, A. Imamura, H. Fujimoto, H. Yamamoto and H. Inokuchi, *Phys. Scr.*, 1990, **41**, 167.
23 T. Gumpenberger, J. Heitz, D. Bäuerle and T. Rosenmayer, *Appl. Phys. A*, 2005, **80**, 27–33.
24 G.-J. Zhao, B. H. Northrop, K.-L. Han and P. J. Stang, *J. Phys. Chem. A*, 2010, **114**, 9007–9013.
25 Y. Li, F. Li and Z. Chen, *J. Am. Chem. Soc.*, 2012, **134**, 11269–11275.
26 X. Li, L. Liu and H. B. Schlegel, *J. Am. Chem. Soc.*, 2002, **124**, 9639–9647.
27 D. Kang, H. Y. Lee, J.-H. Hwang, S. Jeon, D. Kim, S. Kim and S.-W. Kim, *Nano Energy*, 2022, **100**, 107531.
28 N. A. Lanzillo and C. M. Breneman, *J. Phys.: Condens. Matter*, 2016, **28**, 325502.
29 W. Zhao, J. Ding, Y. Zou, C.-a. Di and D. Zhu, *Chem. Soc. Rev.*, 2020, **49**, 7210–7228.
30 A. Shimizu, Y. Ishizaki, S. Horiuchi, T. Hirose, K. Matsuda, H. Sato and J.-i. Yoshida, *J. Org. Chem.*, 2020, **86**, 770–781.
31 P. Morvillo and E. Bobeico, *Sol. Energy Mater. Sol. Cells*, 2008, **92**, 1192–1198.
32 G. L. Eakins, J. S. Alford, B. J. Tiegs, B. E. Breyfogle and C. J. Stearman, *J. Phys. Org. Chem.*, 2011, **24**, 1119–1128.
33 J. L. Teunissen, F. De Proft and F. De Vleeschouwer, *J. Chem. Theor. Comput.*, 2017, **13**, 1351–1365.
34 C. H. Liu, M. R. Niazi and D. F. Perepichka, *Angew. Chem., Int. Ed.*, 2019, **58**, 17312–17321.
35 C.-H. Liu, A. Wei, M. F. Cheung and D. F. Perepichka, *Chem. Mater.*, 2022, **34**, 3461–3467.
36 D. Chen, Y. Liu, C. Xia, Y. Han, Q. Sun, X. Wang, W. Chen, X. Jian, W. Lv and J. Ma, *InfoMat*, 2022, **4**, e12247.
37 Z. B. Muche, Y. Nikodimos, T. M. Tekaligne, S. K. Merso, T. Agnihotri, G. G. Serbessa, S.-H. Wu, W.-N. Su and B. J. Hwang, *Chem. Eng. J.*, 2023, **476**, 146400.
38 S. R. Chaudhari, S. Mogurampelly and N. Suryaprakash, *J. Phys. Chem. B*, 2013, **117**, 1123–1129.
39 T. Steiner, *Angew. Chem., Int. Ed.*, 2002, **41**, 48–76.
40 H. Wang, J. H. Hsu, G. Yang and C. Yu, *Adv. Mater.*, 2016, **28**, 9545–9549.
41 J.-H. Hsu and C. Yu, *Nano Energy*, 2020, **67**, 104282.
42 K. Seki, R. Mitsumoto, E. Itoc, T. Araki, Y. Sakurai, D. Yoshimura, H. Ishii, Y. Ouchi, T. Miyamae and T. Narita, *Mol. Cryst. Liq. Cryst. Sci. Technol., Sect. A*, 2001, **355**, 247–274.
43 K. Nagayama, T. Miyamae, R. Mitsumoto, H. Ishii, Y. Ouchi and K. Seki, *J. Electron. Spectrosc. Relat. Phenom.*, 1996, **78**, 407–410.
44 B. Alchagirov, L. K. Afaunova, F. Dyshekova and R. K. Arkhestov, *Tech. Phys.*, 2015, **60**, 292–299.
45 P. A. Anderson, *Phys. Rev.*, 1949, **75**, 1205.
46 J. Hong, J. Yoon, J.-W. Park, Y.-C. Ha, J. Lee and I. Hwang, *J. Power Sources*, 2025, **655**, 237925.
47 R. Tao, B. Steinhoff, C. H. Sawicki, J. Sharma, K. Sardo, A. Bishtawi, T. Gibbs and J. Li, *J. Power Sources*, 2023, **580**, 233379.
48 D. L. Pugmire, C. J. Wetteland, W. S. Duncan, R. E. Lakis and D. S. Schwartz, *Polym. Degrad. Stab.*, 2009, **94**, 1533–1541.
49 L. Ignat'eva and V. Buznik, *Russ. J. Gen. Chem.*, 2009, **79**, 677–685.
50 H. Oh, G.-S. Kim, B. U. Hwang, J. Bang, J. Kim and K.-M. Jeong, *Chem. Eng. J.*, 2024, **491**, 151957.
51 J. Kim, K. Park, M. Kim, H. Lee, J. Choi, H. B. Park, H. Kim, J. Jang, Y. H. Kim and T. Song, *Adv. Energy Mater.*, 2024, **14**, 2303455.
52 H. Kim, J. H. Lim, T. Lee, J. An, H. Kim, H. Song, H. Lee, J. W. Choi and J. H. Kang, *ACS Energy Lett.*, 2023, **8**, 3460–3466.
53 J. K. Koo, J. Lim, J. Shin, J. K. Seo, C. Ha, W. T. A. Ran, J.-H. Lee, Y. Kwon, Y. M. Lee and Y.-J. Kim, *Energy Storage Mater.*, 2025, 104270.
54 J. Wang, D. Shao, Z. Fan, C. Xu, H. Dou, M. Xu, B. Ding and X. Zhang, *ACS Appl. Mater. Interfaces*, 2024, **16**, 26209–26216.
55 S. Jessl, D. Beesley, S. Engelke, C. J. Valentine, J. C. Stallard, N. Fleck, S. Ahmad, M. T. Cole and M. De Volder, *Mater. Sci. Eng., A*, 2018, **735**, 269–274.
56 R. Tao, B. Steinhoff, X.-G. Sun, K. Sardo, B. Skelly, H. M. Meyer III, C. Sawicki, G. Polizos, X. Lyu and Z. Du, *Chem. Eng. J.*, 2023, **471**, 144300.